# From Ligand- to Metal-centered Reactivity: Metal Substitution Effect in Thiosemicarbazone-based Complexes for H 2 Production

Alexandre Barrozo, Maylis Orio

# From Ligand- to Metal-centered Reactivity: Metal Substitution Effect in Thiosemicarbazone-based Complexes for $H_2$ Production

Alexandre Barrozo* and Maylis Orio*

Aix-Marseille Univ., CNRS, Centrale Marseille, iSm2, Marseille, France.
E-mail: alexandre.hernandes-barrozo@univ-amu.fr; maylis.orio@univ-amu.fr

Supporting information for this article is given via a link at the end of the document.

**Abstract:** The quest to develop and optimize catalysts for $H_2$ production requires a thorough understanding in the possible catalytic mechanisms involved. Transition metals are very often the centers of reactivity in the catalysis, although this can change in the presence of a redox-active ligand. Investigating the differences in catalysis when considering ligand- and metal-centered reactivity is important to find the most optimal mechanisms for hydrogen evolution reaction. Here, we investigated this change of reactivity in two versions of a thiosemicarbazone-based complex, using Co and Ni metal centers. While the Ni version has a ligand-centered reactivity, Co switches it toward a metal-centered one. Comparison between the mechanisms show differences in rate-limiting steps, and shows the importance of identifying those steps in order to optimize the system for hydrogen production.

## Introduction

Over the past decades, the scientific community has been striving to create molecular electrocatalysts that can be used on industrial scale for mass production of hydrogen. One of the main challenges has been the development of catalysts that rely solely on earth-abundant metals. For that, hydrogenases[1-3] have been an important template, with attempts being made to either reproduce the active site architecture of these enzymes (biomimetic),[4-9] or to create catalysts that follow the same kind of reactivity (bioinspired),[10-13] which is essentially metal-centered.

Recently, a new class of homogeneous catalysts based on thiosemicarbazone ligands have emerged.[14-20] They are promising candidates due to their efficiency, low overpotential requirement and the potential for a ligand-centered reactivity. By ligand-centered, we mean that the ligand will store and transfer electrons and protons for the hydrogen evolution reaction (HER).This property offers new degrees of freedom for designing new catalysts, for instance, facilitating the use of substituent effects.[20,21,22]

In the quest to better understand how thiosemicarbazone catalysts work, we studied the effects of metal substitution using DFT calculations. We considered a cobalt (CoTSC) version[19] of the previously studied NiTSC[20,23]. Nevertheless, available experimental data to validate our calculations differ in the choice of the acid with triethylamine ($Et_3NH^+$) for CoTSC and trifluoric acid (TFAH) for NiTSC.[20] So we also considered the effect of different proton source to make such comparison. Here, we show the main differences between Co and Ni as metal centers in the catalysis of HER, and show how metal substitution can change the center of reactivity from the TSC ligand (for Ni) to the metal center (for Co). Our calculations suggest that this mechanistic shift changes the rate limiting step of the catalytic cycle. Additionally, while it is expected that a stronger acid will be better for HER, we justify this result by comparing the free energy profiles of proton transfer from these two acids.

## Results and Discussion

### CoTSC and axial ligands

Fig. 1 shows the X-ray structure obtained for CoTSC.[19] Note that the obtained structure is a dimer with an $NCS^-$ anion bound to each Co center. While the bound anions originate from the synthesis of the complex, the dimeric formation could be an artifact from the conditions for crystallization.[19] There are a few questions that arise here: does the dimeric form hold upon substitution and throughout the catalytic cycle? Does the $NCS^-$ ligand remains bound to Co for CoTSC in its monomeric form, or will it dissociate upon reduction? And can $NCS^-$ be exchanged by

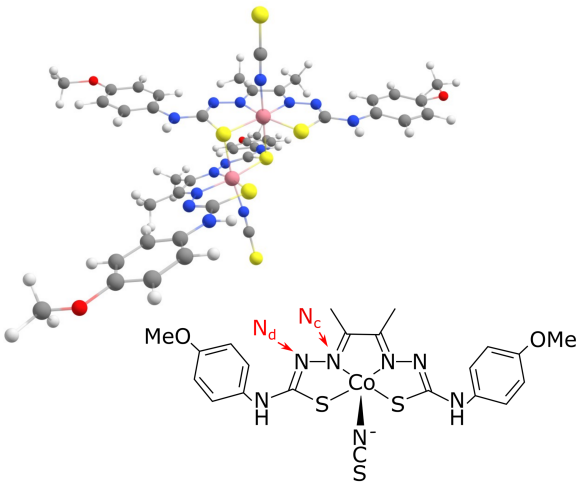


**Figure 1.** Representation of the dimer of CoTSC-$NCS^-$ obtained from X-ray diffraction.[19] In red text, we indicate the notation adopted for this article, where $\mathbf{N_c}$ corresponds to the coordinating N atoms, and $\mathbf{N_d}$ is the distal N atom further away from Co.

a solvent molecule? To answer them, we need to calculate the free energy difference between the dimeric and two monomeric forms, as well as estimate the free energies associated with the dissociation of $NCS^-$. To do so, we must determine the charge and spin multiplicity of CoTSC in its monomeric form, with and without $NCS^-$. Thus, we started by comparing the free energies for different oxidation states with distinct spin multiplicities.

Following conclusions from our previous study,[19] the catalytic cycle starts with a $Co^{III}$ center. We initially wanted to identify the most favorable oxidation states for each monomeric unit. For that, we performed calculations considering the possible binding of an additional solvent molecule to $Co^{III}$, resulting in an octahedral geometry. Geometry optimizations show that the additional solvent molecule dissociates for the triplet state, while it remains bound for the singlet state. We then calculated the free energy difference between these two states, finding a ~1 kcal·mol$^{-1}$ preference for the singlet state (Table S1). Although the difference is small, the complex in its monomeric form is more likely to be found in an octahedral singlet state. As for the first reduced state, it should be a doublet. In this case, geometry optimizations show that the solvent molecule dissociates, while $NCS^-$ remains bound, yielding a pentacoordinated species. Finally, for the second reduced state we have an open-shell singlet. Finally, a third reduction yields a doublet (Table S1). With that information, we can proceed with answering the questions above.

The first one involves dimer *vs.* two monomers. Free energy calculations with $NCS^-$ as the axial ligand show that while there is a preference of 2.7 kcal·mol$^{-1}$ for the monomers when the complex is neutral, the difference jumps to 15.5 kcal·mol$^{-1}$ upon the first reduction (Table S2). This energetic preference means that it is very likely that a dissociation of the dimer will occur. In fact, the optimized geometries of the dimer show that, while in the neutral case the dimer we have the Co-S being both 2.29 Å, these distances change upon the first reduction, with one of the Co-S distances going to 2.32 Å, and the other at 2.96 Å. Finally, we calculated the reduction potential for the first reduction of the dimer, yielding -1.13 V (*vs.* $FeCp^{+/0}$). This is far from the first reduction potential obtained experimentally, -0.60 V, which is better reproduced by calculations on the monomer alone (see next section). Thus, we will proceed with the analysis of CoTSC as a monomer only.

For the second question, we analyzed the binding energies of axial ligands at distinct oxidation states. We initially start with the system at an octahedral geometry. We then performed potential energy surface (PES) scans to study the energy profile associated with $NCS^-$. The scans were used to obtain approximate transition state structures for ligand dissociation. Then, geometry optimization was used to obtain the structures for the bound and dissociated ligand, and we obtained free energy differences through harmonic analysis. This process was considered for distinct oxidation states (see Table 1 and Fig. S2). For the unreduced complex, we clearly see an unfavorable dissociation free energy ($\Delta G$) for $NCS^-$, which would likely implicate a tall barrier for dissociating it from the Co center. Thus, no dissociation is likely to occur within the timescale associated with the HER, which is 130 s$^{-1}$.[19] However, $\Delta G$ drops significantly upon the first reduction, with barriers getting no taller than 10 kcal·mol$^{-1}$. As we shall see later on, while the first reduction will involve the dissociation of a solvent molecule, changing the complex from an octahedral to a pentacoordinated system, the low barrier for dissociation of $NCS^-$ can cause another ligand dissociation, and this is backed by comparing experimental and calculated electrochemical data. Finally, for the second reduction, $\Delta G$ is further lowered, with a slight increase in the activation barrier. An additional set of calculations was performed substituting $NCS^-$ by DMF, to consider a potential ligand exchange effect. We observe similar results, with DMF being a weaker ligand.

**Table 1.** Estimation of dissociation free energies ($\Delta G_{nth}$, for the nth reduction), and activation free energies for dissociation of the axial ligands ($\Delta G^{\ddagger}_{nth}$). Values estimated from optimized structures with ligand connected and disconnected. All results are in kcal·mol$^{-1}$.

| Ligand | $\Delta G_{0th}$ | $\Delta G_{1st}$ | $\Delta G^{\ddagger}_{1st}$ | $\Delta G_{2nd}$ | $\Delta G^{\ddagger}_{2nd}$ |
|---|---|---|---|---|---|
| $NCS^-$ | 16.7 | 1.7 | 9.0 | -2.2 | 10.4 |
| DMF | 9.5 | -1.5 | 2.8 | -9.2 | 1.4 |

To summarize, there is an energetic advantage for having monomers over dimers, and theoretical calculations of the redox potentials for the monomers are in better agreement with experimental data. Regarding $NCS^-$, it is unlikely it will dissociate prior to any reduction. However, this becomes a possibility upon reduction. If we are to estimate the timescale for dissociating $NCS^-$ using Transition-State Theory (Eyring's equation for a transmission coefficient of one[24]), kinetic rates of $NCS^-$ dissociation are of the order of ~$10^6$ s$^{-1}$ after the first reduction, and ~$10^5$ s$^{-1}$ after two subsequent reductions. Such values are at least three orders of magnitude above the rates of HER for this complex. As we shall see, dissociation of the ligand leads to better agreement between experimental and calculated redox potentials of CoTSC in the presence of $Et_3NH^+$.

### The first catalytic steps of CoTSC: (E)EC

HER is a sequence of steps that can be classified as electrochemical (denoted as E, where the complex is reduced), chemical steps (denoted as C, where the complex is protonated), and can even involve concerted electron-proton steps ([EC]), as seen in NiTSC.[23] To find which step comes first, we started by inspecting the reduction potentials for CoTSC considering the absence and presence of axial ligand ($NCS^-$ and DMF). We mentioned previously that it is likely that any bound axial ligand would dissociate upon reduction due to low activation barriers. Here, we will show that this also makes sense when comparing experimental[19] and theoretical electrochemical data. We started with the same $Co^{III}$ monomeric state as previously discussed, and considered three subsequent reduction events, in line with what was observed from available voltammetry experimental data.[19]

Table 2 shows the results, with the best agreement between calculated and experimental data highlighted. Such agreement can be explained considering the following pathway (Fig. 2): (a) CoTSC starts with axial ligands $NCS^-$ and DMF which is expected from the synthesis protocol and ligand field theory;[19] (b) the first reduction occurs (-0.70 V, in agreement with the experimental -0.60 V), triggering DMF dissociation. From there, we can also expect a second dissociation (c), involving $NCS^-$, which now beco-

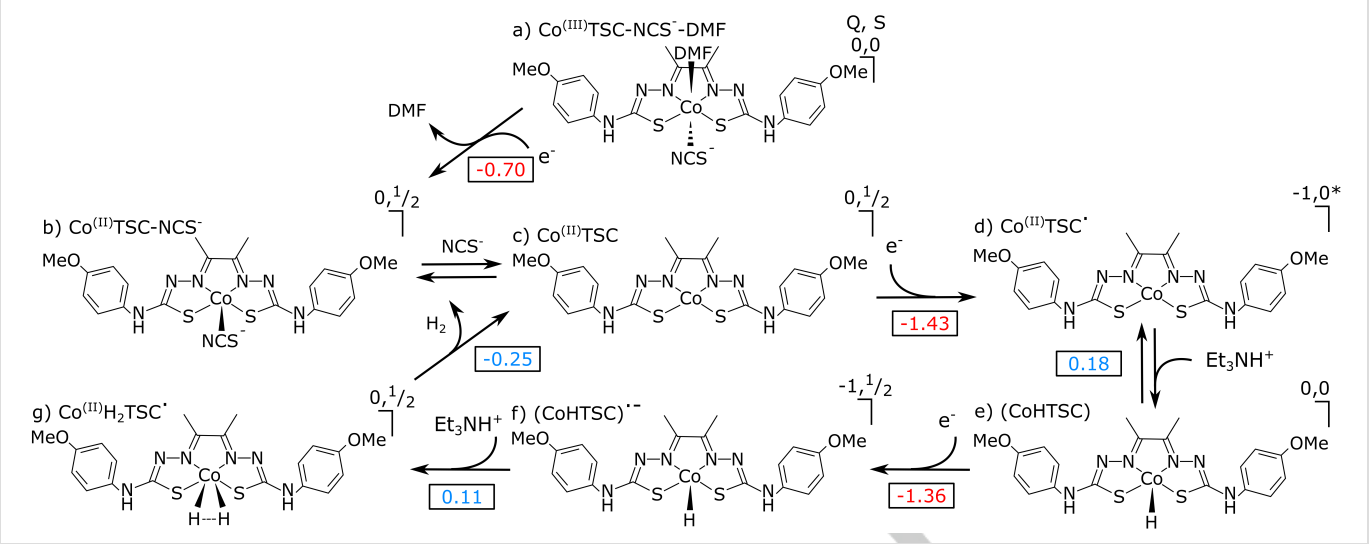


**Figure 2.** HER catalytic cycle of CoTSC in presence of $Et_3NH^+$. Oxidation states determined based on previous work[19] and analysis of singly occupied MOs and population analysis (see Figure S1 and Table S3). States e and f have no precise oxidation state assignment due to delocalization of the electronic structure and no substantial change in charge in the Co center. Red numbers correspond to redox potentials, and blue numbers, free energy differences for proton transfer reactions, both in eV. Numbers on top of each state corresponds to its charge and spin state. For the latter, a value of 0* corresponds to an open-shell singlet, obtained from BS-DFT (see Experimental Section and SI for details).

mes weakly bound. This can be explained due to the low barrier of 9 kcal·mol$^{-1}$ for dissociation of $NCS^-$, and the fact that reducing CoTSC with $NCS^-$ a second time (-1.77 V) is energetically more expensive than without it (-1.43 V). After $NCS^-$ release (c), the second reduction occurs. We also performed calculations for a third reduction for sake of comparison with experiments. Such reduction is likely to occur without any axial ligand, since now it either requires more voltage to reduce a CoTSC-NCS complex, or that it is energetically unfavorable for DMF to bind to CoTSC to profit from its less negative reduction potential (Table 1).

To visualize the electronic structure of CoTSC upon reduction, we plotted spin densities at each oxidation state (Fig. 3), starting with the initial neutral state with $NCS^-$, after the first and second reductions (for the third reduction, we considered protonation of Co, see discussion below). When comparing to NiTSC, it is possible to see a clear distinction between how these two systems accommodate electrons particularly at the first reduction, with NiTSC having the tendency to form a radical ligand, whereas CoTSC holds most of its density in the metal center. However, upon the second reduction of CoTSC, there is a ligand radical formation, forming an open-shell singlet state. As we shall see later on, Co will be the main proton acceptor, where $H_2$ production will take place.

**Table 2.** Redox potentials for the first, second and third reductions of the CoTSC complex in the absence of $Et_3NH^+$, compared with previous results for NiTSC.[23] Redox potential values are *vs.* FeCp (4.87 V), in V. Highlighted data shows the best agreement with CV experiments.

| | CoTSC | | | NiTSC | |
|---|---|---|---|---|---|
| **Ligand** | $E^0_{1st}$ | $E^0_{2nd}$ | $E^0_{3rd}$ | $E^0_{1st}$ | $E^0_{2nd}$ |
| None | 0.00 | -1.43 | -2.36 | -1.54 | -2.29 |
| $NCS^-$ | -0.70 | -1.77 | -3.04 | | |
| DMF | -0.44 | -1.73 | -2.18 | | |
| Exp.[19] | -0.60 | -1.48 | -2.48 | -1.57 | -2.20 |

Based on what we have so far, and comparing to data for hydrogen production obtained for an applied voltage of -1.7 V,[19] it is possible to have up to two subsequent reductions. The first reduction is a $Co^{III}$ to $Co^{II}$ step, and brings the catalyst to the beginning of the HER. This step will be denoted here as '(E)', to describe it as a preparation step. Figure 2 shows that this step is skipped when multiple cycles take place, with the cycle restarting at a $Co^{II}$ state (b, Fig. 2). While two subsequent reduction steps fit experimental data, it is important to confirm if this is the case by checking whether proton transfer events can occur before, in between, or after these two reductions. Cyclic voltammetry experiments considering various concentrations of $Et_3NH^+$ show no shift in redox potentials compared to experiments performed in the absence of acid.[19] Thus, there is no stabilization effect occurring as seen for NiTSC in the presence of TFAH.[20,23] While this data alone is already pointing toward an (E)E-sequence as our first steps, we can confirm this hypothesis with the help of DFT calculations.

First, we need to know where protons can be attached to in CoTSC. From Figure 1, and as previously justified in our previous

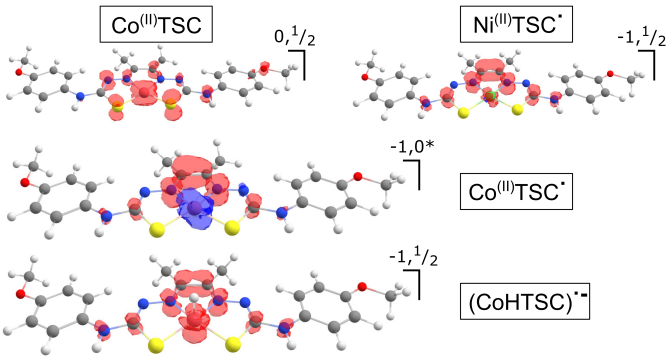


**Figure 3.** Spin densities of CoTSC after first reduction with NCS- released (top), for the second reductions (middle), and for the third reduction considering the first protonation of the complex (bottom). We compare spin densities for the first reduction with its NiTSC counterpart.

study of CoTSC[19] and NiTSC,[23] we will consider four potential protonation sites: Co, S, $N_c$ and $N_d$, all sitting near the center of the complex. Table 3 shows the relative $pK_a$ values against the $pK_a$ of $N_d$ considering three possible redox states, from the neutral CoTSC case, where $NCS^-$ is initially bound, to up to two subsequent reductions. We see that there is a preference for protonating $N_d$ for the initial state and after the first reduction. However, this preference changes to Co once the second reduction occurs. This is in contrast to NiTSC, where $N_d$ is the energetically most favorable site for all its oxidation states.[23]

We then investigated the proton transfer between $Et_3NH^+$ and CoTSC. We placed $Et_3NH^+$ in position for a H-bonding interaction that leads to proton transfer for different oxidation states, as performed for NiTSC with TFAH.[23] For the initial state and after the first reduction, we placed $Et_3NH^+$ within H-bond distance with one of the $N_d$ atoms. We included $NCS^-$ for the two initial states, and removed it when accounting for the complex after the second reduction. For each oxidation state, we considered the reactant (CoTSC + $Et_3NH^+$) and product states (CoTSC-H + $Et_3N$) of the proton transfer event. Then we proceeded with geometry optimization calculations to assess the equilibrium structures for the two reaction states (a and b, Fig. 2). During the geometry optimization, the proton bounces back to form $Et_3NH^+$ in both product states. This suggests that such reaction yields a high-energy state, meaning their formation is energetically unfavorable. However, when we considered the second reduction state, where now Co is the protonation state, such issue does not occur, indicating that this product state is now stable, *i.e.* after two subsequent reductions, or the (E)E steps.

To evaluate the energetics associated with this proton transfer to Co, we performed a 2-D potential energy surface (PES) scan considering the N-H distance from $Et_3NH^+$, and Co-H distance, constraining them at 7x7 distinct distances. Fig. 4 shows the surface, displaying an associative mechanism (see also Table 34). Our methodology was not sufficient to properly capture the transition state for this reaction. Thus, the analysis presented here remains qualitative. Nevertheless, the PES suggests this proton transfer does not possess a potential energy barrier. Additionally, we are neglecting quantum effects of the reaction, such as proton delocalization and tunneling. In principle, those effects facilitate proton transfer. Thus, we can expect this proton transfer to be rather fast, thus not becoming rate-limiting.

Finally, we calculated the free energy difference between product and reactant states of the proton transfer, obtaining a $\Delta G_0$ of 4.2 kcal·mol$^{-1}$. The endergonic nature of this reaction, together with an activation barrier that is not high, renders it reversible, creating a step that competes with the catalytic mechanism of HER. For instance, an activation free energy of ~10 kcal·mol$^{-1}$ (similar to our activation potential energy) for a forward reaction would mean an activation of ~6 kcal·mol$^{-1}$ for the backward reaction. Using Eyring's equation gives us rates of $3.2\times10^5$ s$^{-1}$ for the forward, and $2.7\times10^8$ s$^{-1}$ for the reverse proton transfer. This is an important aspect of the kinetics in the catalytic cycle, as reversibility will slow the process.

**Table 3.** Relative $pK_a$s of the four protonation sites *vs.* $N_d$. Results shown for three states (see Fig. 2): a) neutral, with NCS- bound, b) after the first reduction, and c) second reduction events, considering $NCS^-$ departure. Negative results indicate lesser likelihood of protonation compared to $N_d$.

| | Catalytic cycle state | | |
|---|---|---|---|
| **Site** | **a** | **b** | **c** |
| $N_d$ | 0.0 | 0.0 | 0.0 |
| $N_c$ | -17.0 | -19.1 | -6.8 |
| S | -8.8 | -9.6 | -6.8 |
| Co | -16.3 | -11.1 | 3.0 |

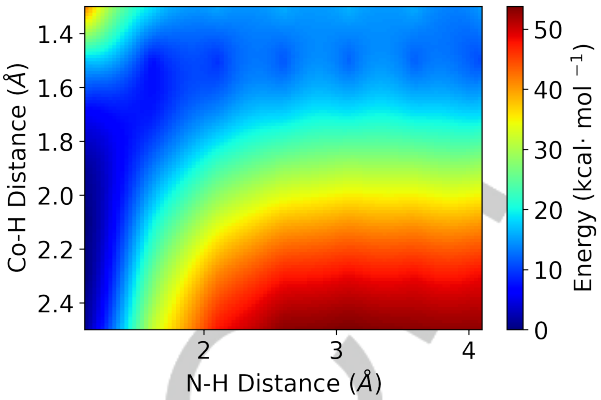


**Figure 4. Top**: 2-D potential energy surface scan for the first proton transfer phenomenon, from $Et_3NH^+$ to the Co atom after two subsequent reductions of CoTSC.

## The (E)ECEC cycle: final steps

Our calculations suggest that the first steps of the catalytic cycle are (E)EC, the first of which involving the dissociation of $NCS^-$. To investigate the last steps of the cycle, we performed similar calculations as those performed for the first steps. The simplest hypothesis at first is to include a second proton, and assess the energetics of $H_2$ formation, as if the cycle would form a (E)ECC mechanism. To investigate this possibility, we calculated the relative $pK_a$s of the protonation sites involved. Since protonation occurred at the Co, the symmetry of the system did not change, so we have only four sites to investigate: Co, S, $N_c$ and $N_d$. Results are shown in Table 4. As we see, $N_d$ is again the most favorable candidate for protonation in a (E)ECC mechanism. However, when considering the presence of $Et_3NH^+$ in H-bonding interaction with one of the $N_d$ atoms in the complex, we saw the same issue as discussed for the first proton transfer: geometry optimization for the product state resulted in the transferred proton bouncing back to $Et_3N$. Thus, the catalytic cycle would encounter difficulties to perform this process.

A second hypothesis would be to include a third reduction of the system, after the first protonation. This means that the catalytic mechanism would reach an (E)ECEC-type of cycle. To assess the viability of this third reduction, we performed free energy calculations for the third reduction process with CoTSC protonated at the Co center. We obtained -1.36 V, close to the -1.43 V calculated for the second reduction before any protonation. Both processes could appear as a single feature in a cyclic voltammetry experiment in the presence of a proton source.[19]

**Table 4.** Relative $pK_a$s of the four protonation sites *vs.* $N_d$ for the second protonation event, considering the Co as already protonated. Results shown for two oxidation states, following convention from Fig. 2: after the second reduction and first protonation to Co (d), and following a third reduction event (e). Negative results indicate lesser likelihood of protonation compared to $N_d$.

| | Catalytic cycle state | |
|---|---|---|
| **Protonated Sites** | **d** | **e** |
| Co, $N_d$ | 0.0 | 0.0 |
| Co, $N_c$ | -16.8 | -8.1 |
| Co, S | -8.6 | -8.3 |
| Co, Co | -8.6 | 5.3 |

Thus, an (E)ECEC sequence can be described by the experimental and theoretical data.

If we consider a third reduction, the second proton transfer would preferably take place at the Co atom (Table 4). Thus, Co could hold two protons in close proximity for $H_2$ formation. To test this hypothesis, we performed geometry optimization calculations of the reactant and product states for the proton transfer to Co, in which both protons would be in close proximity. Geometry optimization calculations converge for stable reactant and product states. Thus, we proceeded with probing the energetics of this second proton transfer, as performed for the previous case. Due to the possibility of $H_2$ formation already at this point, we chose to perform a PES scan for different H-H distances. At $H_2$ equilibrium distance, both protons remain bound to Co. Results are shown in Fig. 5 and Table S5. We obtained a similar PES shape, with a $\Delta G_0$ of 2.4 kcal·mol$^{-1}$ between reactant and product states. The lower free energy difference would translate into a less reversible reaction compared to the first proton transfer reaction.

To finalize the cycle, we need to know the free energies associated with the release of $H_2$ from the Co center. We performed a PES constraining two distances, which correspond to Co-H for each proton (Table S6). The PES shows a very shallow peak, with a reaction free energy different $\Delta G_0$=-5.7 kcal·mol$^{-1}$. Thus, $H_2$ release is likely to be a fast and favourable process. Even if the second proton transfer turns out to be reversible, where a competition between the forward and backward reaction exists, that should not hinder $H_2$ formation.

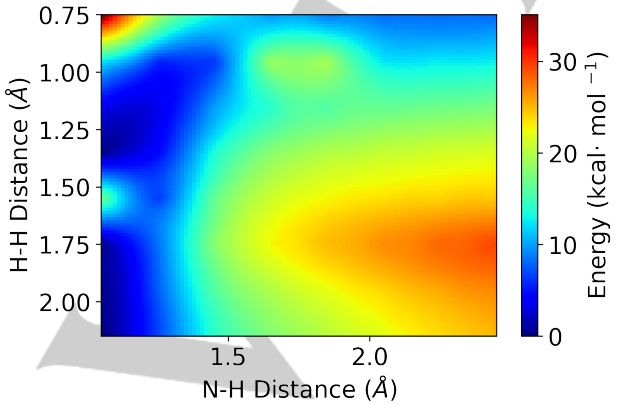


**Figure 5.** 2-D potential energy surface scan for the second proton transfer phenomenon, from $Et_3NH^+$ to the H atom attached to Co after the (E)ECE steps.

### $H_2$ formation and overall kinetics

Our results suggest an (E)ECEC mechanism, but due to the fact that the first step is an activation step that will be skipped for subsequent cycles, we focus the discussion in the last four steps: ECEC. There are three main observations worth highlighting: i) both electron transfer processes occur with similar potential requirements; ii) both proton transfer reactions possess low activation barriers, with positive $\Delta G_0$ values to the point that the reverse proton transfer reaction will be above one order of magnitude faster than the forward one; iii) $H_2$ release is a fast process with $\Delta G_0$ below -5 kcal·mol$^{-1}$, indicating that it will significantly favor the release of $H_2$, ending the catalytic cycle. Since our calculations are performed in an implicit solvent, we cannot estimate the kinetics of diffusion for the acid forming a H-bonding interaction with the complex. In this discussion, we shall omit diffusion, although we acknowledge that it could be playing a role in limiting overall cycle.

To localize the rate-limiting step of this catalytic cycle, let us write the kinetic reaction equations, following notation from Fig. 2:

$$\mathbf{c)}\ \mathbf{Co^{II}TSC} + e^- \rightarrow \mathbf{Co^{II}TSC^{\bullet -}}$$

$$\mathbf{d)}\ \mathbf{Co^{II}TSC^{\bullet -}} + \mathbf{Et_3NH^+} \rightleftarrows (\mathbf{Co^{\overset{+}{H}}HTSC})^{\bullet -} + \mathbf{Et_3N}$$

$$\mathbf{e)}\ (\mathbf{Co^{\overset{+}{H}}(\overset{+}{H})HTSC})^{\bullet} + e^- \rightarrow (\mathbf{CoHTSC})^{\bullet -}$$

$$\mathbf{f)}\ (\mathbf{Co^{\overset{+}{H}}(\overset{+}{H})TSC})^{\bullet -} + \mathbf{Et_3NH^+} \rightleftarrows \mathbf{Co^{II}(H_2)TSC^{\bullet}} + \mathbf{Et_3N}$$

Previous experimental work on $H_2$ production of CoTSC with $Et_3NH^+$ was performed with a voltage of -1.6 V *vs.* $FeCp^{+/0}$ applied to the system. This is about 0.2 V more negative than both electrochemical steps (c and e), and thus slightly more than the required for those steps to occur. Calculating electron transfer rates is a rather complex task, as we would need to account for the electronic coupling between CoTSC and the electrode used in the experiment, as well as the reorganization free energies. These are issue that will be addressed in future work. For the proton transfer reactions (d and f), each will have two rate constants, corresponding to a forward and reverse motion of the proton. We previously gave the example of an activation free energy of 10 kcal·mol$^{-1}$. In this case, the first proton transfer, 'c', will have $k_{c,F}$=3.2×10$^5$ s$^{-1}$ and $k_{c,R}$=2.7×10$^8$ s$^{-1}$ for forward and reverse directions, respectively. Regardless of the real activation free energy, we will always find a ratio between these two reaction rates of $k_{c,F}/k_{c,R}$~10$^{-3}$. As long as this proton transfer barrier does not surpass ~15 kcal·mol$^{-1}$, this reaction will not be a rate-limiting step.

Due to the faster rate for the reverse direction for the first proton transfer, it leads to the formation of pre-equilibrium states. In this case, we can consider steady-state kinetics processes for this step, with an equilibrium constant of: $K_c=k_{c,F}/k_{c,R}$~10$^{-3}$. One can show that the overall kinetic rate constant of a reaction following a pre-equilibrium event is given by the product between the pre-equilibrium constant K and the rate constant of the following step.[22] In the case of our ECEC mechanism, we have a first pre-equilibrium between the first proton transfer reaction 'c'

and the second electron transfer 'd'. This makes the overall kinetic rate for the second electron transfer to become, $k=K_c k_d=10^{-3}\times k_d$. Thus, even if this electron transfer reaction is fast, the pre-equilibrium state from the first proton transfer reaction can impact its rate. Although the same logic can be applied for the second proton transfer, 'e', we note that $H_2$ production and release is fast enough to compete with the reverse proton transfer reaction.

Thus, it is possible to say that one of the key steps that are slowing down the reaction is the reversibility of the first proton transfer, which is responsible for a $10^{-3}$ factor included in the overall kinetic rates. While we could not pinpoint the exact rate-limiting step for CoTSC, our study suggests that it is not related to proton transfer reactions, which is the case for NiTSC.[23] Finally, it is worth mentioning that everything we presented here concerns $Et_3NH^+$. The use of a stronger acid such as TFAH could help amend for the reversibility seen in the proton transfer reactions. Nevertheless, it is also possible that the mechanism changes. There are several questions that remain to be addressed.

## Conclusion

We presented a mechanistic analysis of the catalytic cycle of CoTSC in the presence of $Et_3NH^+$ and TFAH, and compared it with our previous studies of NiTSC. We started by investigating the effects of a $NCS^-$ ligand attached to the Co center. By comparing DFT calcualtions with cyclic voltammetry experiments, we concluded that it should not play any role throughout the HER. We probed multiple combinations of electrochemical and chemical steps, and showed the overall catalytic cycle is best described by a (E)ECEC sequence, where the first step (E) is an activation of the complex, in which reduction leads to release of $NCS^-$ release. Analysis of electronic structure and energetics of proton transfer reactions show that the catalytic cycle of CoTSC is metal-centered, unlike the ligand-centered reactivity seen for NiTSC.

Our calculations suggest that both proton transfer reactions should not possess rate-limiting activation barriers. The first proton transfer is particularly succeptible to reversiblity due to high $\Delta G_0$ in favour of leaving $Et_3N$ protonated. Due to this, pre-equilibrium states will be formed, causing a loss of up to three orders of magnitude of the kinetics for the subsequent step, which is the final electrochemical step. While it is possible that this last electron transfer could be the rate-limiting step, we would need to accurately assess the activation barriers of the proton transfers, investigate each electron transfer step, as well as the diffusion of the complex and acid to allow us to pinpoint the rate-limiting step for CoTSC. We believe that this work open several questions that need to be addressed not only for this system, but for any homogeneous catalyst for the HER.

## Acknowledgements

The authors gratefully acknowledge financial support of this work by the ANR (ANR-19-CE05_0030_01).

**Keywords:** Hydrogen • Hydrogen production • Catalysis • DFT • Metal Substitution

[1] J. C. Fontecilla-Camps, A. Volbeda, C. Cavazza, Y. Nicolet, *Chem. Rev.*, **2007**, *107*, 4273–4303.
[2] K. A. Vincent, A. Parkin, F. A. Armstrong, *Chem. Rev.*, **2007**, *107*, 4366-4413
[3] W. Lubitz, H. Ogata, O. Rudiger, E. Reijerse, *Chem. Rev.*, **2014**, *114*, 4081-4148.
[4] M. L. Helm, M. P. Stewart, R. M. Bullock, M. R. DuBois, D. L. DuBois, *Science,* **2011**, *333*, 863.
[5] M. Y. Darensbourg, E. J. Lyon, J. J. Smee, *Coord. Chem. Rev.* **2000**, *206*, 533–561;
[6] T. B. Rauchfuss, *Acc. Chem. Res.* **2015**, *48*, 2107–2116;
[7] Z. Li, Y. Ohki, K. Tatsumi, *J. Am. Chem. Soc.* **2005**, *127*, 8950–8951;
[8] K. Weber, T. Kramer, H. S. Shafaat, T. Weyhermuller, E. Bill. M. van Gastel, F. Neese, W. Lubitz, *J. Am. Chem. Soc.* **2011**, *141*, 472-481
[9] D. Brazzolotto, M. Gennari, N. Queyriaux, T. R. Simmons, J. Pocault, S. Demeshko, F. Meyer, M. Orio, V. Artero, C. Duboc, *Nat. Chem.* **2016**, *8*, 1054–1060;
[10] H. I. Karunadasa, C. J. Chang, J. R. Long, *Nature***, 2010**, *464*, 1329-1333
[11] M. Ravazet, V. Artero, M. Fontecave *Inorg. Chem.*, **2005**, *44*, 4786-4795
[12] P. Zhang, M. Wang, Y. Yang, T. Yao, L. Sun *Angew. Chem.* **2014**, *53*, 13803-13807
[13] E. J. Thompson, L. A. Berben, *Angew. Chem.*, **2015**, *54*, 11642-11646
[14] X. Jing, P. Wu, X. Liu, L. Yang, C. He, C. Duan, *New J. Chem.*, **2015**, ***39***, 1051
[15] W. R. McNamara *et al.*, *Dalton Trans.*, **2015**, ***44***, 14265
[16] A. Z. Haddad, B. D. Garabato, P. M. Kozlowski, R. M. Buchanan, C. A. Grapperhaus, *J. Am. Chem. Soc.*, **2016**, ***138***, 7844.
[17] A. Z. Haddad, S. P. Cronin, M. S. Mashuta, R. M. Buchanan, C. A. Grapperhaus, *Inorg. Chem.*, **2017**, ***56***, 11254
[18] T. Straistari, J. Fize, S. Shova, M. Réglier, V.Artero, M. Orio, *Chem. Cat. Chem.,* **2017**, *9,* 2262
[19] T. Straistari, R. Hardré, J. Fize, S. Shova, M. Réglier, V. Artero, M. Orio, *Chem. Eur. J.*, **2018**, ***24***, 8779
[20] M. Papadakis, A. Barrozo, T. Straistari, N. Queyriaux, A. Putri, J. Fize, M. Giorgi, M. Réglier, J. Massin, R. Hardré and M. Orio. *Dalton Trans.*, **2020**, *49*, 5064-5073.
[21] G.-G. Luo, H.-L. Zhang, Y.-W. Tao, Q.-Y. Wu, D. Tian and Q. Zhang. *Inorg. Chem. Front.*, **2019**, *6,* 343-354.
[22] M. Drosou, F. Kamatsos and C. A. Mitsopoulou, *Inorg. Chem. Front.,* **2020**, *7*, 37-71
[23] A. Barrozo and M. Orio. *RSC Adv.*, **2021**, 11 (9), 5232-5238
[24] P. Atkins, J. De Paula and J. Keeler. *Atkins' Physical Chemistry*, 11th ed., Oxford University Press, **2017**.

## Entry for the Table of Contents

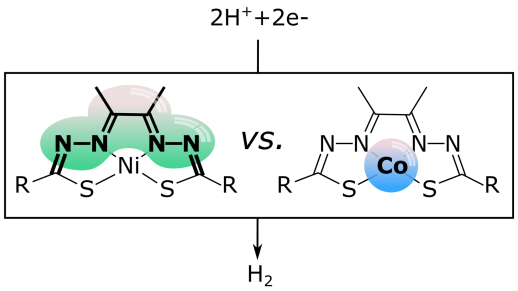


Certain homogeneous catalysts for $H_2$ production can have either transition metals or redox-active ligands as their center of reactivity. Investigating the differences in catalysis when considering ligand- and metal-centered reactivity is important to find the most optimal mechanisms for hydrogen evolution reaction. Here, we show how changing between Co and Ni metal centers in a thiosemicarbazone complex can affect the reactivity of the system. While the Ni version has a ligand-centered reactivity, Co switches it toward a metal-centered one. Comparison between the mechanisms show differences in rate-limiting steps, and shows the importance of identifying those steps in order to optimize the system for hydrogen production.